BISTRO：なぜ今サブミリ波偏波観測なのか

長谷川哲夫
（国立天文台チリ観測所）

偏波の発生

Intrinsicな偏波

1. 電荷の加速度運動→電磁波
   電荷の運動方向の不均一→偏波
   例：ダイポールアンテナの放射、シンクロトロン放射、整列ダストによる熱放射
2. 磁場中の原子・分子による吸収・放出
   例：ゼーマン効果、メーザー、Goldreich-Kylafis効果

Radiative transferによって発生・変化する偏波

3. 散乱
   例：反射・散乱による直線偏波の発生、多重散乱による円偏波の発生
4. 選択的吸収・散乱
   例：ワイヤグリッドによる偏波分離、整列ダストによる吸収・散乱
5. プラズマ中の電磁波伝搬
   例：ファラデー回転

偏波による整列ダストの観測

可視光・赤外線（選択的吸収・散乱）

利点

- 背景が事実上点源のため、無限に細い視線に沿った測定が可能
- 希薄な星間雲でも高精度の測定が可能

弱点

- 高密度星間雲では減光が大きいため背景星が少なく、空間サンプリングが急激に粗くなる

サブミリ波（ダスト熱放射のintrinsicな偏波）

利点

- 高密度星間雲の観測が得意
- 高密度星間雲でもサブミリ波では光学的に薄い

弱点

- 望遠鏡のビーム内で平均した姿
- 感度の限界（地上観測）
- 分解能の限界（衛星観測）

偏波による整列ダストの観測

可視光・赤外線（選択的吸収・散乱）
サブミリ波（ダスト熱放射のintrinsicな偏波）

共通する弱点

- 前提となるダストの整列機構の理解が不完全
  - Davis-Greensteinメカニズム（1951、常磁性ダスト粒子の熱的スピン）→ ×
  - DGメカニズムの修正（超磁性ダスト、超熱的スピン、H_2形成の反跳）→ ×
  - Radiative torqueメカニズム（Dolginov & Mytrophanov 1976、1990年代にDraineらが再発見、ダスト形状のhelicityによる左右円偏波の吸収の差によりスピン）→ ○（今のところは）
- 磁場の3次元構造のうち視線に垂直な成分のみ
  - 方向はわかる（視線に沿った平均）
  - 強度の推定は間接的（Chandrasekhar-Fermi法）

ダストの整列と偏波効率

THE ASTROPHYSICAL JOURNAL, 674:304–315, 2008 February 10

THE EFFICIENCY OF GRAIN ALIGNMENT IN DENSE INTERSTELLAR CLOUDS: A REASSESSMENT OF CONSTRAINTS FROM NEAR-INFRARED POLARIZATION

D. C. B. WHITTET,[1] J. H. HOUGH,[2] A. LAZARIAN,[3] AND THIEM HOANG[3]
Received 2007 October 12; accepted 2007 October 31

ABSTRACT

We present the results of a detailed study of interstellar polarization efficiency (as measured by the ratio p_λ/τ_λ) toward molecular clouds, with the aim of discriminating between grain alignment mechanisms in dense regions of the interstellar medium. The data set includes both continuum measurements in the K (2.2 μm) passband and values based on ice and silicate spectral features. Background field stars are used to probe polarization efficiency in quiescent regions of dark clouds, yielding a dependence on visual extinction well-represented by a power law ($p_\lambda/\tau_\lambda \propto [A_V]^{-0.52}$), in agreement with previous work. No significant change in this behavior is observed in the transition region between the diffuse outer layers and dense inner regions of clouds, where icy mantles are formed, and we conclude that mantle formation has little or no effect on the efficiency of grain alignment. The field-star data are used as a template for comparison with results for embedded young stellar objects (YSOs). The latter generally exhibit greater polarization efficiency compared with field stars at comparable extinctions, some displaying enhancements in p_λ/τ_λ by factors of up to ~6 with respect to the power-law fit. Of the proposed alignment mechanisms, that based on radiative torques appears best able to explain the data. The attenuated external radiation field appears adequate to account for the observed polarization in quiescent regions for extinctions up to $A_V \sim 10$ mag. Radiation from the embedded stars themselves may enhance alignment in the lines of sight to YSOs. Enhancements in p_λ/τ_λ observed in the ice features toward several YSOs are of greatest significance, as they demonstrate efficient alignment in cold molecular clouds associated with star formation.

Subject headings: dust, extinction — infrared: ISM — ISM: magnetic fields — polarization

ダストの整列と偏波効率

Whittet+2008

Background field stars

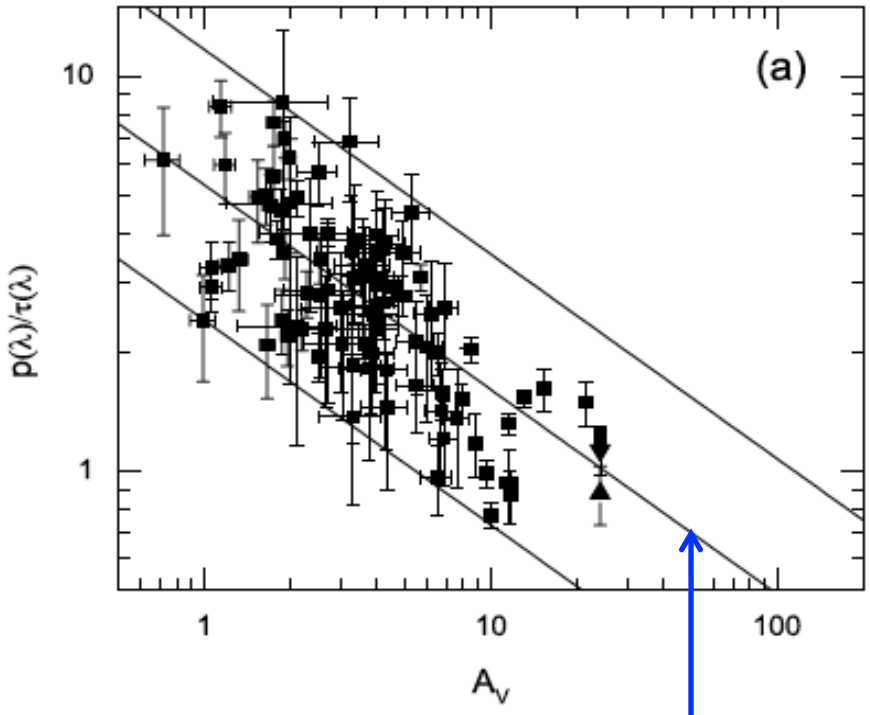

Embedded YSOs

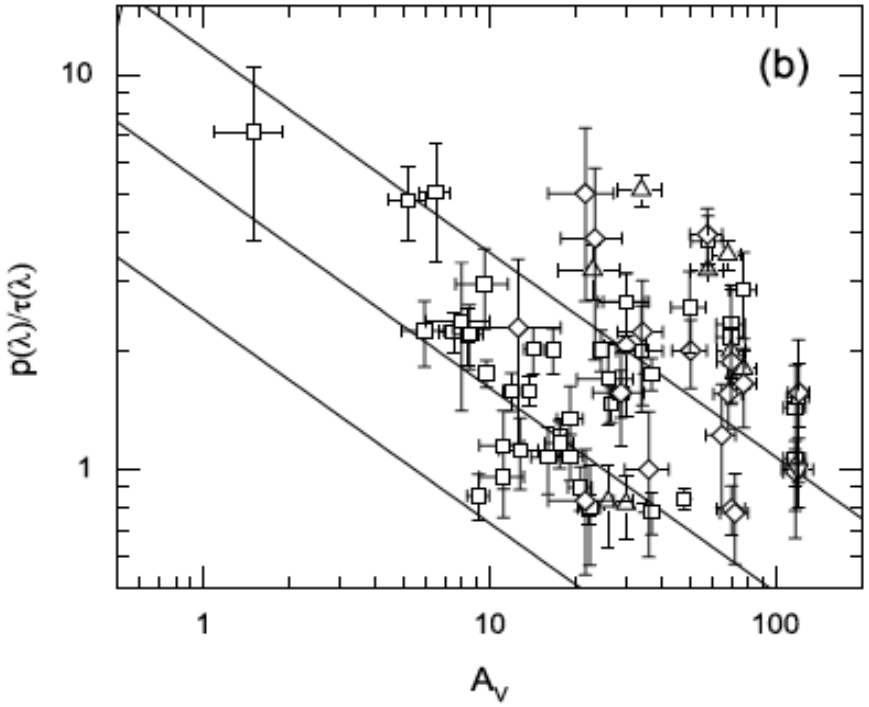

Regression line fitted to the Taurus field star data

ダストの整列と偏波効率

The Astronomical Journal, 149:31 (8pp), 2015 January doi:10.1088/0004-6256/149/1/31

GRAIN ALIGNMENT IN STARLESS CORES

T. J. Jones[1,5], M. Bagley[1,5], M. Krejny[2,5], B.-G. Andersson[3], and P. Bastien[4]
[1] Minnesota Institute for Astrophysics, University of Minnesota, Minneapolis, MN 55455, USA; tjj@astro.umn.edu
[2] Cree Inc., 4600 Silicon Dr., Durham, NC, USA
[3] SOFIA Science Center, USRA, Moffett Field, CA, USA
[4] Centre de recherche en astrophysique du Québec and Département de Physique, Université de Montréal, Montréal, Canada
Received 2014 September 8; accepted 2014 November 15; published 2014 December 24

ABSTRACT

We present near-IR polarimetry data of background stars shining through a selection of starless cores taken in the K band, probing visual extinctions up to $A_V \sim 48$. We find that P_K/τ_K continues to decline with increasing A_V with a power law slope of roughly −0.5. Examination of published submillimeter (submm) polarimetry of starless cores suggests that by $A_V \gtrsim 20$ the slope for P versus τ becomes ∼−1, indicating no grain alignment at greater optical depths. Combining these two data sets, we find good evidence that, in the absence of a central illuminating source, the dust grains in dense molecular cloud cores with no internal radiation source cease to become aligned with the local magnetic field at optical depths greater than $A_V \sim 20$. A simple model relating the alignment efficiency to the optical depth into the cloud reproduces the observations well.

Key words: dust, extinction – ISM: clouds – ISM: magnetic fields

Jones+2015

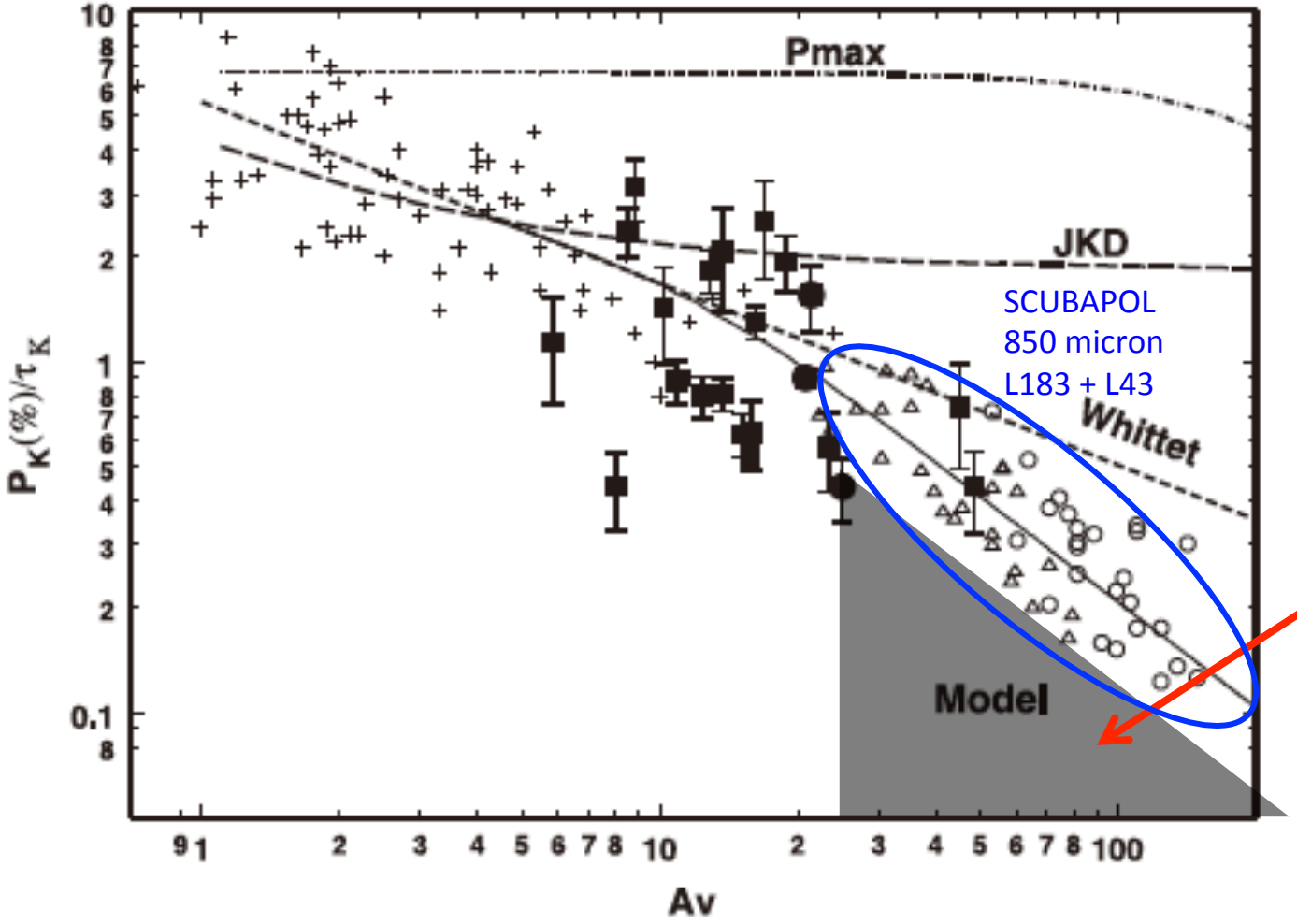

注意！

ダイナミックレンジの限られたデータから、*pl*/d*pl*が大きいデータ点のみを選別すると、人工的な傾向を作ってしまう

Figure 5. Same as Figure 2, with the addition of submm observations and a simple model fit to the trend at high extinctions. The L183 data is plotted as open triangles and the L43 data as open circles. Each submm data set was shifted vertically by an arbitrary amount to line up with the *K* band data (see Appendix B). The solid line is the result of a simple model where the alignment of the grains decreases as a function of optical depth into the cloud.

偏波による整列ダストの観測

可視光・赤外線（選択的吸収・散乱）

利点

- 背景が事実上点源のため、無限に細い視線に沿った測定が可能
- 希薄な星間雲でも高精度の測定が可能

弱点

- 高密度星間雲では減光が大きいため背景星が少なく、空間サンプリングが急激に粗くなる

サブミリ波（ダスト熱放射のintrinsicな偏波）

利点

- 高密度星間雲の観測が得意
- 高密度星間雲でもサブミリ波では光学的に薄い

弱点

- 望遠鏡のビーム内で平均した姿
- 感度の限界（地上観測）
- 分解能の限界（衛星観測）

JCMTのSCUBA-2/POL-2やALMAによる高感度・高解像観測でブレークスルー

Ser-emb 8
Hull+2017

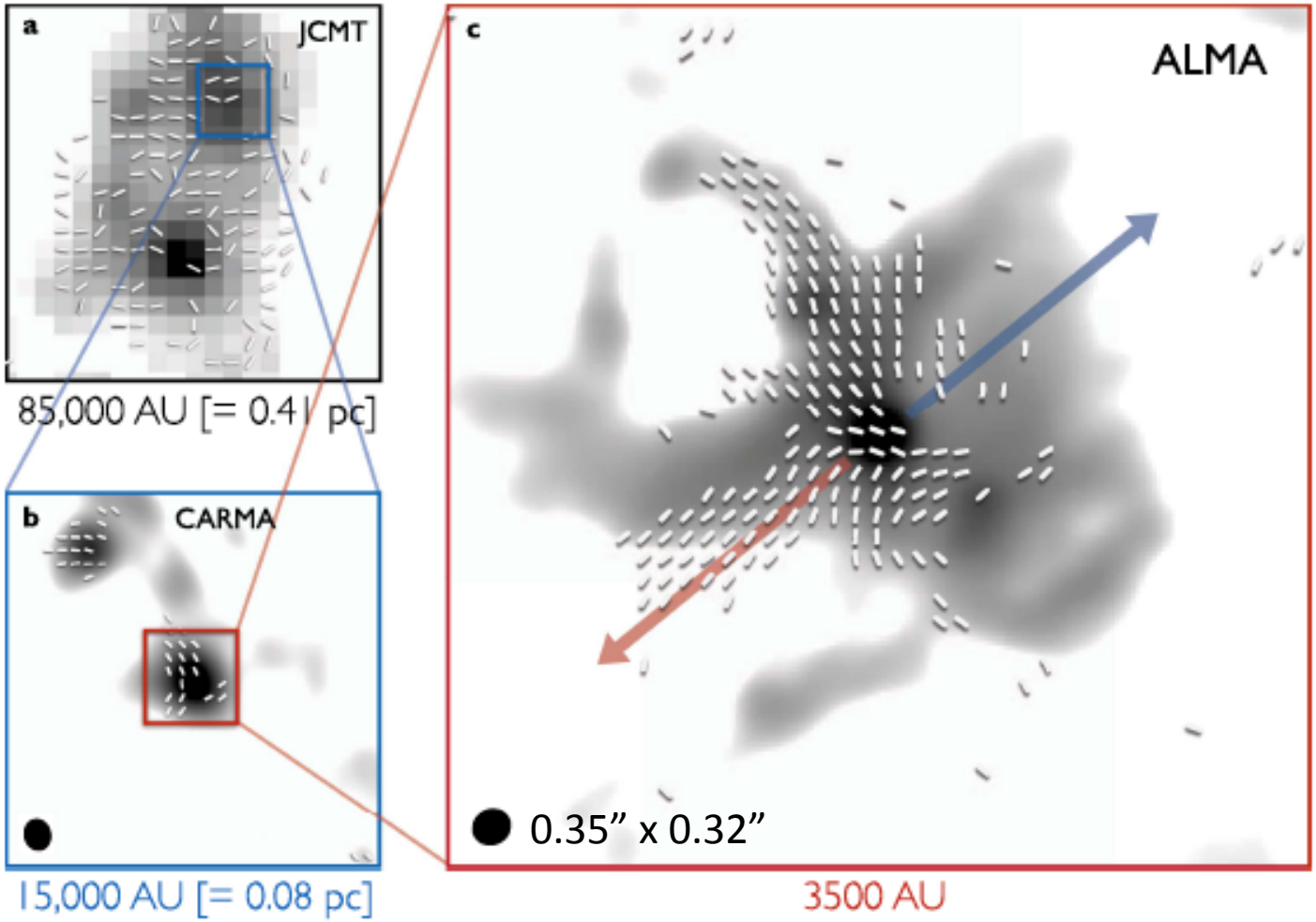

Figure 1. Multi-scale view of the magnetic field around Ser-emb 8 (α_{J2000} = 18:29:48.089, δ_{J2000} = +1:16:43.32). Line segments represent the magnetic field orientation, rotated by 90° from the dust polarization (the length of each segment is identical and does not represent any other quantity). Grayscale is total intensity (Stokes *I*) thermal dust emission. Panel (a) shows 870 μm JCMT observations (Matthews et al. 2009), (b) shows 1.3 mm CARMA observations (Hull et al. 2014), and (c) shows 870 μm ALMA observations, revealing the magnetic field morphology with ~10,000, 1000, and 140 au resolution, respectively. For the ALMA data, line segments are plotted where the polarized intensity $P > 3\sigma_P$; the rms noise in the polarized intensity map σ_P = 25 μJy beam^{-1}. The dust emission is shown starting at 3 × σ_I, where the rms noise in the Stokes *I* map σ_I = 50 μJy beam^{-1}. The peak polarized and total intensities in the ALMA data are 0.693 mJy beam^{-1} and 102 mJy beam^{-1}, respectively (the two peaks do not coincide exactly). The red and blue arrows indicate the redshifted and blueshifted lobes of the bipolar outflow (Hull et al. 2014). The text below each of the panels indicates the physical size of the image at the 436 pc distance to the Serpens Main region (Ortiz-León et al. 2017; see earlier results by Dzib et al. 2010, 2011). The black ellipses in the lower left corners of the ALMA and CARMA maps represent the synthesized beams (resolution elements). The ALMA beam measures 0.″35 × 0.″32 at a position angle of −63°; the CARMA beam measures 2.″89 × 2.″43 at a position angle of 13°. The JCMT data have a resolution of 20″.

(The data used to create this figure are available.)

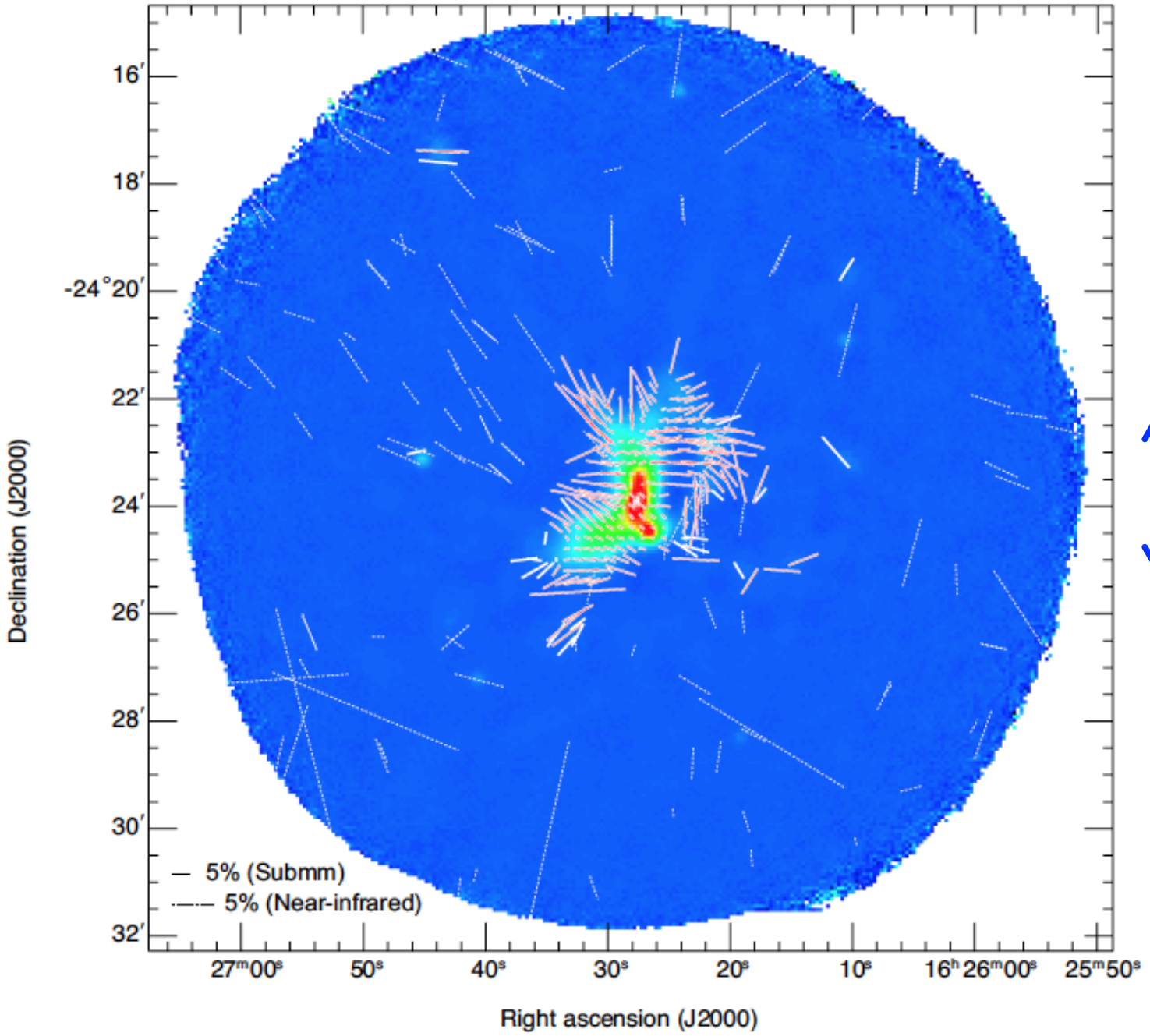

BISTRO
Rho Oph A
Kwon+2018

10,000 AU
= 0.05 pc

Figure 5. Same as Figure 3 but rotated by 90° with near-infrared polarization vectors (white dotted vectors) from Kwon et al. (2015). Scale vectors of 5% at submillimeter and near-infrared wavelengths are shown in the bottom left corner.

BISTRO 850 micron (B direction)
Kwon+2018

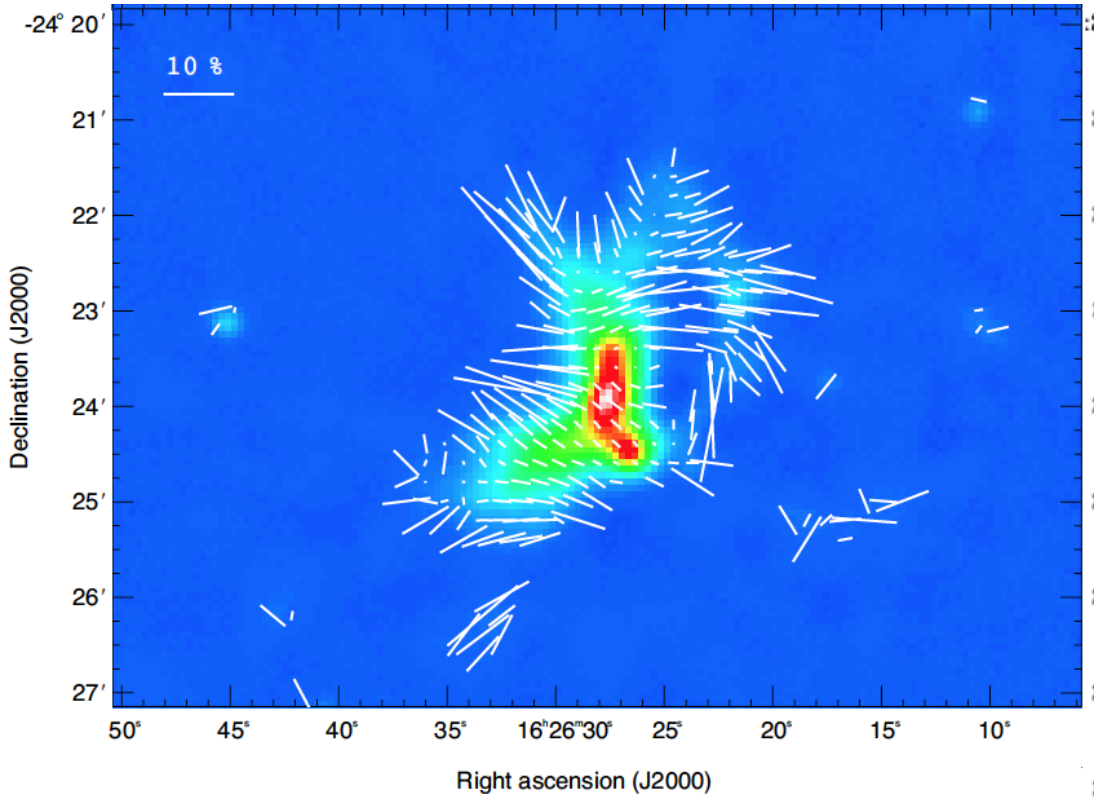

SCUBAPOL 850 micron (E direction)
Mattheus+2009

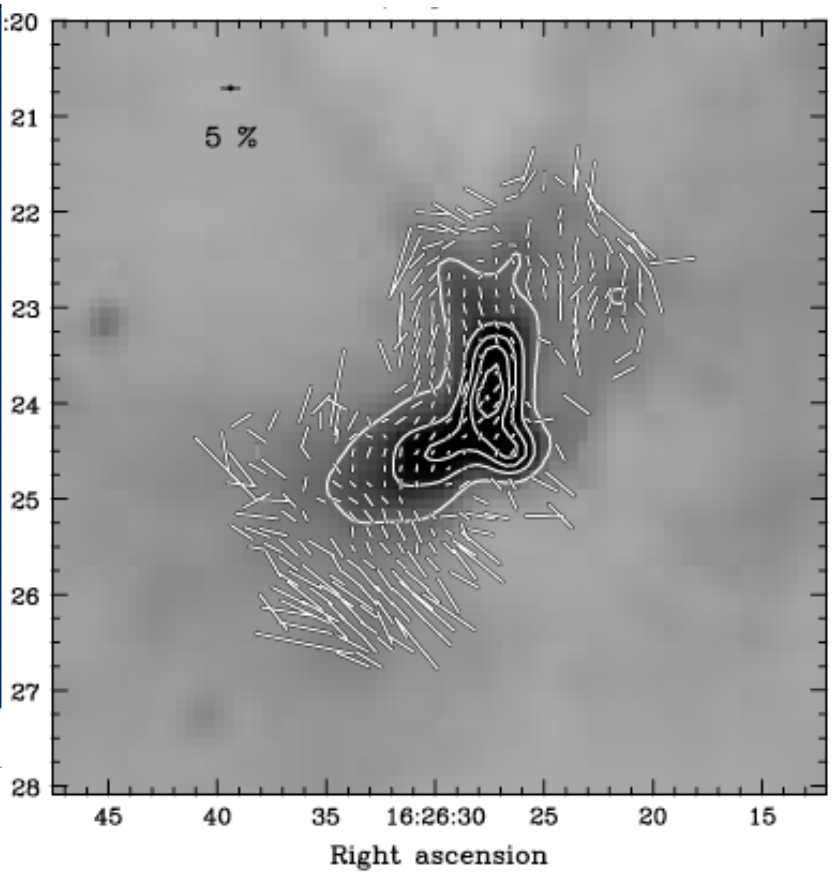

SCUBAPOLでも外側まで偏波ベクトルを書いていたが、
BISTROのデータは信頼性が大幅に向上している

BISTRO

Rho Oph A

Kwon+2018

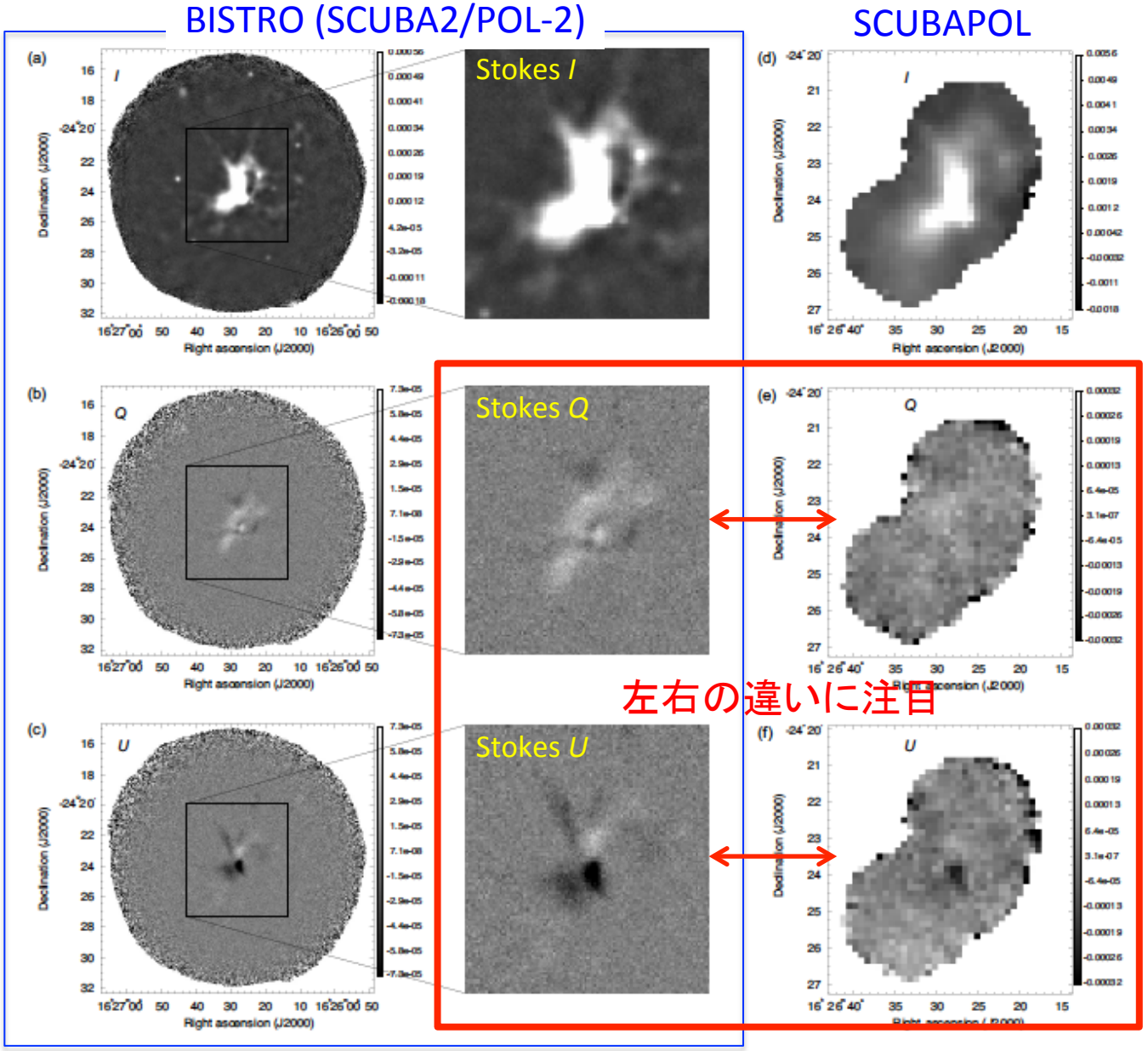

Figure 2. SCUBA-2/POL-2 data (this work) compared with SCUPOL (previous work). The intensity gray scales are different between the POL-2 and SCUPOL data. (a)–(c) Stokes I, Q, and U images (linear scale) of the ρ Oph-A core region obtained with the JCMT with SCUBA-2/POL-2. The Stokes Q and U images (b and c) have the same gray scale in picowatt (pW) units. The SCUPOL field of view (d)–(f) is indicated by a black box in Figures 2(a)–(c), respectively. (d)–(f) 850 μm Stokes I, Q, and U images of the ρ Oph-A core region obtained from the JCMT with SCUPOL (from The SCUBA Polarimeter Legacy Catalogue). The Stokes Q and U images (e and f) have the same gray scale in volts units (see Matthews et al. 2009).

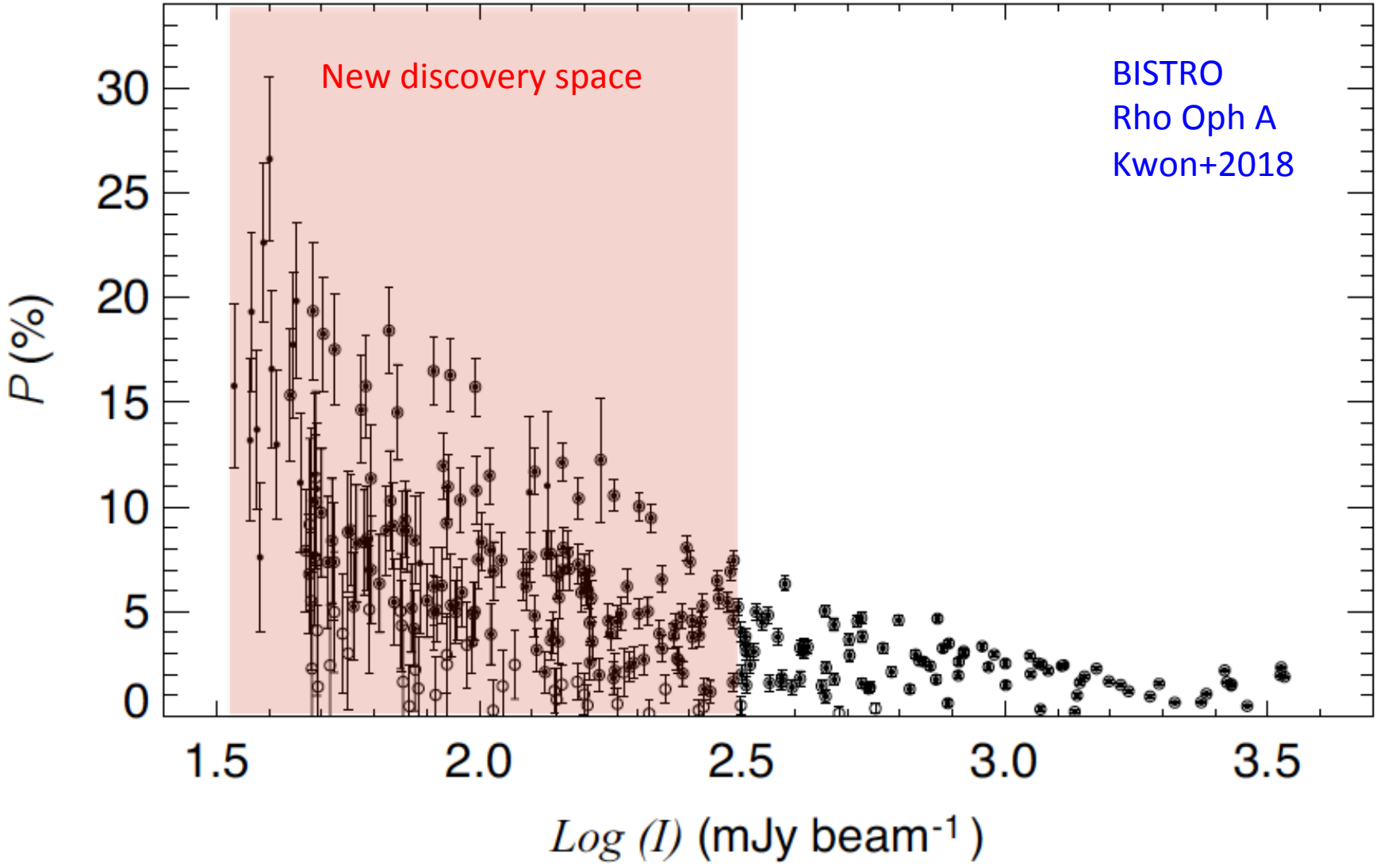

Figure 7. Degree of polarization (P) vs. Intensity (I). Unfilled circles: $I > 0$, $I/\delta I > 20$, and $P > 0$. Filled circles: $I > 0$, $P/\delta P > 2$, and $\delta P < 4\%$. Double circles: Overlap between unfilled and filled circles.

観測される偏波率の解釈例

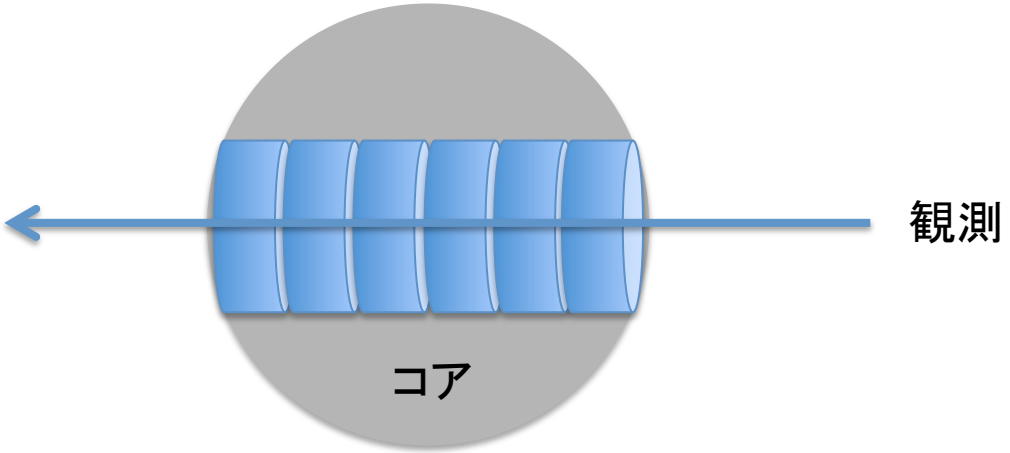

個々のスラブ
- 強度 I_0 および偏波効率 p_0 は同じ
- 偏波の向きは独立

N個のスラブを重ねて見ると（光学的に薄い場合）
- 観測される $I_{obs} = I_0 N$
- 観測される（Q_{obs}, U_{obs}）は、個々のスラブの（Q, U）のベクトル和
  → $p_{obs} I_{obs} = (Q^2_{obs} + U^2_{obs})^{0.5} \sim p_0 I_0 N^{0.5}$
- 観測されると期待される偏波率 $p_{obs} = p_0 N^{-0.5}$

BISTRO + ALMA

ブレークスルー

- BISTRO
  - 高い感度とダイナミックレンジでコア周辺部まで磁場構造を正確に描くことができる
    （0.05-0.1 pc @120 pc；近赤外偏光観測と接続）
  - 幅広い偏波率（<1% – 20%）が有意に測定される
- ALMA偏波観測
  - 高い空間分解能と感度でコアの中心領域の複雑な磁場構造を描くことができる
  - コアの中心領域でも高い偏波率が観測される